Construction and Building Materials 438 (2024) 137099

Contents lists available at ScienceDirect

Construction and Building Materials

journal homepage: www.elsevier.com/locate/conbuildmat

Characterization of hygrothermal, gas pressure and stress characteristics for poplar wood during unilateral surface densification

Zhipeng Zhu [a,1], Xiaoxue Song [a,1], Xiang Chi [a], Jingyao Zhao [a], Qiaofang Zhou [b], Antoni Sanchez-Ferrer [c,*], Dengyun Tu [b,*], Wanli Cheng [a,*]

[a] Key Laboratory of Bio-based Material Science and Technology of Ministry of Education, Northeast Forestry University, Harbin 150040, China
[b] Key Laboratory of Bio-based Materials and Energy, Ministry of Education, South China Agricultural University, Guangzhou 510642, China
[c] Chair of Wood Science, TUM School of Life Sciences, Technical University of Munich, Winzererstr. 45, Munich 80797, Germany

ARTICLE INFO

Keywords:
Unilaterally surface-densified
Gas pressure analysis
Heat and mass transfer
Stress-strain

ABSTRACT

Unilateral surface compression in wood presents notable benefits, including reduced wood volume loss and energy consumption, rendering a highly promising and extensive utilization. However, shortcomings in compressed wood arise due to unclear gas pressure, temperature, and moisture content distribution within the wood during hot pressing. In this paper, the temperature and pressure distribution were analyzed utilizing an optical fiber temperature and pressure measurement system within the wood during hot pressing. Moreover, the moisture content, stress and strain in each layer at the end of hot pressing were discussed extensively. The results showed that the wood surface layer (SL) and subsurface layer (SSL) maximum temperature values were similar even with different layer thicknesses. Under sealing conditions, SL and SSL temperatures were generally 6 ℃ to 7 ℃ higher compared to unsealing conditions. The gas pressure maximum value exhibited an opposite order, gradually transferring to the core layer (CL) and declining as the processing time extended. During compression treatment, moisture migrated from the hot end to the cold within the wood. The moisture content displayed significant differences between the middle and end parts of the wood under unsealed conditions, with the disparity becoming more pronounced further away from the hot end. The transition region of the compressed wood served as a stress concentration area, experiencing the highest levels of stress. The dense region followed with the second highest stress levels, while the un-densified region exhibited the least amount of stress. Under the same process parameters, the thickness had little influence on the distribution of dense layers.

1. Introduction

Wood is a biopolymer composite and one of the most sustainable materials capable of carbon sequestration. Its remarkable strength-to-weight ratio and machinability make wood widely applicable as a construction material. With increased eco-consciousness around the world, numerous countries have implemented robust policies and measures to preserve precious timber resources [1,2]. Conversely, these efforts have further exacerbated the persistent imbalance between wood demand and the availability of fresh timber. Thus, a series of innovative approaches have been proposed to address this challenge, such as the efficient utilization of rapidly growing plantation resources.

Fast-growing plantations, such as poplar, often possess relatively low density, poor dimensional stability, and low mechanical strength, which significantly limit their applications [3–5]. In order to optimize the utilization of poplar resources, wood properties are enhanced by treating timber through two effective modification techniques, *i.e.*, chemical impregnation [6,7] and thermo-mechanical densification [8–11]. The latter has notable advantages due to the absence of chemicals and, therefore, more eco-friendly products are obtained, and the use of simple processes where only water and heat are applied. Thermo-mechanical densification includes bulk densification and surface densification [12].

Unilateral surface densification treatment refers to a specific technique that exclusively employs hygrothermal treatment on a specific surface of wooden boards. This method effectively improves the hardness and strength of the treated wood surface while minimizing volume loss [13]. As a result, this process enables the production of premium

* Corresponding authors.
E-mail addresses: sanchez@hfm.tum.de (A. Sanchez-Ferrer), tudengyun@scau.edu.cn (D. Tu), nefucwl@nefu.edu.cn (W. Cheng).
[1] Contributed equally to this work.

https://doi.org/10.1016/j.conbuildmat.2024.137099
Received 23 January 2024; Received in revised form 11 June 2024; Accepted 13 June 2024
Available online 14 June 2024

solid wood products, aligning with the principles of clean and sustainable production. In the process of hot pressing, a rapid accumulation of gas will be present in the wood which can adversely affect the final product performance if the pressure is too high. For instance, excessive gas flow velocities in the reverse direction during continuous pressing can result in blister formation [14], and even a risk of explosion might result when the pressure surpasses the compressive strength limit of the wood tensile strength across the grain [15].

This has a bad effect on product quality and restricts the commercial application of unilateral surface compression wood. The fundamental reason is that heat, moisture and gas pressure migrate from the high-temperature to the low-temperature region during the preparation process, resulting in the uneven distribution of the temperature, moisture and gas pressure inside the wood. Hence, it is crucial to understand the internal gas pressure conditions to prevent or effectively address such issues in plant operations. Additionally, the internal temperature conditions are contingent upon the level of gas pressure. Therefore, accurate gas pressure measurements are necessary for enhancing the understanding of these interactions.

In the conventional process of manufacturing densified wood, the hot press plate is periodically opened during the hot-pressing to release water vapor inside the material. However, this process results in significant heat loss and equipment damage [16]. Consequently, we have devised a simple and efficient temperature differential method for the production of unilateral surface densification compressed wood. Namely, when pressure is applied to both surfaces of the board specimens, only one surface is heated, and the glass transition temperature of the amorphous wood bio-polymers, *i.e.*, lignin, hemicelluloses and amorphous cellulose, is reduced by increasing the moisture content of the heated surface due to a plasticization effect. The heated surface of wood is compressed, while the unheated surface remains largely undeformed. Furthermore, in our previous study, we successfully controlled the thickness and position of the dense layer by controlling the process parameters, *i.e.*, temperature, preheating time, compression speed, compression ratio, and pressure holding time, thereby, achieving accurate regulation of the profile density [17–20]. However, there are still problems and open questions related to the reproducibility of the profile when applying the same process to samples with varying thicknesses.

This paper also presents a comparative analysis to address this question. Moreover, the focus of most researchers lies in studying the variation of gas pressure within artificial panels during hot pressing at present. Thoemen *et al.* [14,21,22] used a steel tube connected to a piezoelectric pressure transducer to determine the gas pressure of wood-fiber mats in a laboratory hot press. Liu *et al.* still used equipment similar to Humphrey to measure internal wood pressure during microwave drying [23]. Their research contributed to the understanding of the events inside wood-based material during hot pressing. However, the above measurement methods involved assessing internal material pressure through pressure transmission tubes connected to external pressure sensors, which inevitably experienced some pressure loss. Furthermore, no further comparative investigations were conducted regarding subsequent material properties. To solve these issues, we have applied an optical fiber pressure and temperature-integrated detection device. The sensor is positioned at the tip of the optical fiber, allowing it to penetrate deep into the material. This design significantly minimized pressure loss while ensuring high resistance to interference for the optical fiber sensor. Although the influence of gas pressure within wood-based panels during the hot pressing process had been discussed years ago, to the best of our knowledge, there has been no research to analyze pressure field distributions during compressed wood production.

This study aims to investigate the alterations in internal temperature and gas pressure, as well as the characteristics of heat transfer and moisture diffusion in wood during the production of unilateral surface densification treatment. Additionally, it aims to reveal the changes in the softening area and location within the wood. The findings of this work might enhance the theoretical system for precise predictive control of the dense layer in unilateral surface densification compressed wood, and offer theoretical underpinning for the development of an advanced technological system for unilateral surface compression of wood.

2. Materials and methods

2.1. Materials preparation

Samples used in this study were produced from poplar wood (*Populus tomentosa Carr.*) which were obtained from Zhoukou (Henan Province, China). The dimensions of the sawn timber followed three specifications: 2100 mm×180 mm×55 mm (L×T×R), 2100 mm×180 mm×45 mm (L×T×R) and 2100 mm×180 mm×35 mm (L×T×R) with 580–620 kg/m^3 air-dried density and 10–16 % initial moisture content. The moisture content was determined according to GB/T 1931–2009, and the average moisture content of the boards was taken as the initial moisture content of these samples and recorded as W_0. Each sawn timber was machined into 4 test boards measuring 400 mm×180 mm (L×T), with a thickness (R) of 30 mm, 40 mm and 50 mm. Test boards without obvious visible defects were selected for subsequent testing (Fig. 1).

Each test board was precisely machined into a sample size of 400 mm×180 mm (L×T). The samples were marked at 5 mm intervals along the thickness direction, with the number of layers denoted as *i*. For instance, when considering a 50 mm thick sample, *i* took an integer value from 1 to 10. The first layer was in contact with the hot end of the hot press (XLB-0.6×0.6 m^3, Jinjiuzhou, China), while the last layer was in contact with the cold end of the hot press. The samples were subjected to boring in the surface layer (SL) (at the position i=1), subsurface layer (SSL) (at the position i=2) and core layer (CL) (at half the thickness) at the medial section. The depth of the boring was precisely half of the sample width (namely 75 mm), to accommodate the positioning of fiber optic temperature and pressure sensors, as shown in Fig. 1, and the resulting weight was measured and recorded as m_0.

To accurately analyze the radial heat and mass transfer behavior of wood during the hot pressing process, sealed and unsealed conditions were employed. When defects such as knots were present, the situation was similar to sealing, and in this condition, the gas pressure inside the sample was considered to reach its maximum value. Consequently, certain samples required sealing treatment. Given that the surface (tangential-section) of samples came into direct contact with the bottom plate of the hot press, only both ends (cross-section) and sides (radial-section) of the sample were sealed. For such a purpose, the epoxy resin E-44 (Hunan Handbrother New Material Co., LTD.) and the hardener $C_4H_{13}N_3$ (AR 99 %, Shanghai Aladdin Biochemical Technology Co., LTD.) were fully mixed at the ratio of 8:1, and evenly applied on the radial section and cross-section of the sample, while being careful to avoid any holes. The sample was left at room temperature until it was completely cured, and the weight the of sample was measured and denoted as m_1.

In order to investigate the influence of moisture content on the internal temperature and gas pressure of wood during the hot pressing process, adjustments were made to the moisture content of the samples. Specifically, three moisture content levels, namely 15 %, 25 %, and 35 %, *i.e.,* wood air-dried condition, critical fiber saturation point condition and above the fiber saturation point condition, were achieved for testing purposes. After the sealing treatment of the samples was completed, procedures for adjusting the moisture content were implemented. The samples that needed to be adjusted to a moisture content of 15 % were placed in a climate chamber (BPC-100CL, Yiheng Scientific Instrument Co., LTD, China) at 28 ℃ and 74 % relative humidity until a stable weight was reached. To attain target moisture contents of 25 % and 35 %, samples were immersed in purified water at a temperature of 50 ℃ until the desired weight was obtained. The moisture content of the samples adjusted to 25 % and 35 % was calculated using Eqs. 1–3:

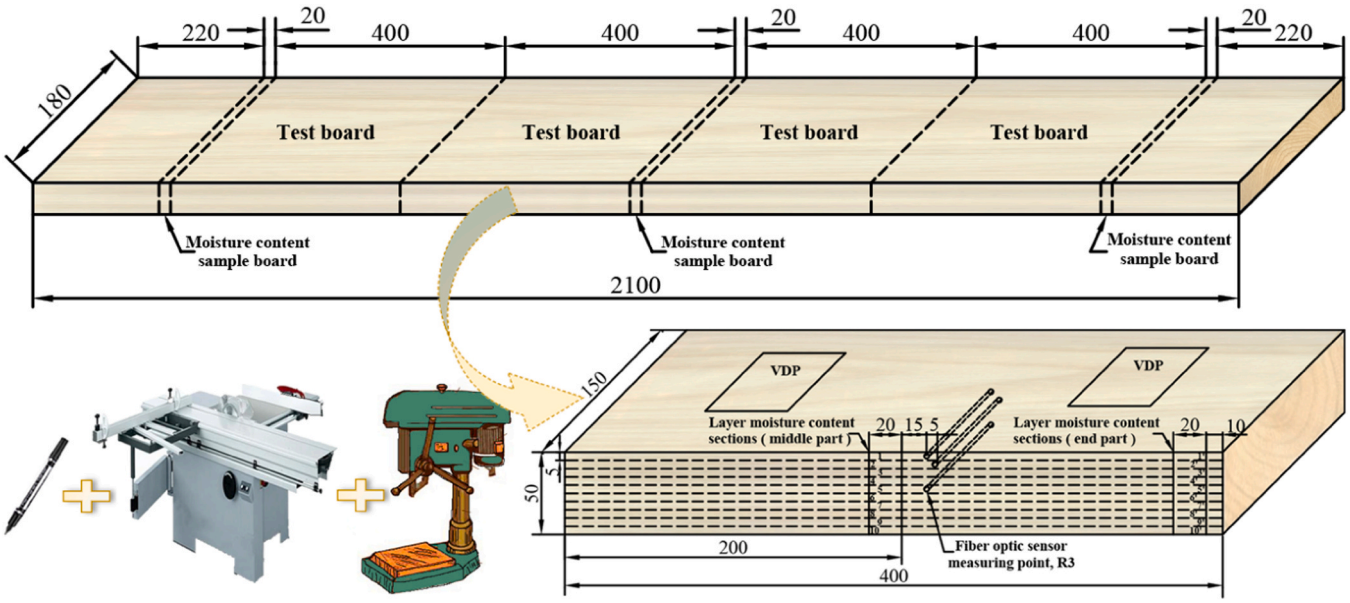

Fig. 1. Sawing and samples marking distribution diagram (take 50 mm thickness as an example).

$$m_t = a \cdot m_{ad} + m_{er} \tag{1}$$

$$m_{ad} = \frac{m_0}{W_0 + 1} \tag{2}$$

$$m_{er} = m_1 - m_0 \tag{3}$$

where m_t is the weight of the sample upon achieving its target moisture content (kg); a is the coefficient with a value of 1.25 and 1.35 for a target moisture content of 25 % and 35 %, respectively; m_{ad} is the absolute dry weight of the sample (kg); m_{er} is the weight of the cured resin on the surface of the sample (kg) - if the sample was not sealed, m_1 is equivalent to m_0, meaning that m_{er} is equal to 0. After reaching the target moisture content, samples were coated with polyethylene film. Subsequent tests could be conducted once the moisture content deviation on the sample thickness was within 3 %, indicating a uniform internal moisture content of the samples.

2.2. Wood densification

The optical fiber pressure and temperature sensors were installed within a pressure-resistant steel pipe measuring 180 mm in length, 4 mm in external diameter, and with a wall thickness of 1 mm. Apart from the top of the steel pipe, which remained open for sensor measurement, the remaining contact area with the sensor transmission line was hermetically sealed using epoxy resin. The sensors were placed in designated positions within the sample, and the gaps between steel pipe and wood were sealed using Teflon tape (Loctite Model 542, Henkel GMBH) and epoxy resin. The exterior surface of the steel pipe was effectively insulated by applying a tightly wrapped layer of insulation cotton. The sensors were connected to a paperless recorder to monitor real-time changes in the internal temperature and gas pressure of the sample.

The preparation process utilized a laboratory-type single-opening hot press (XLB-0.6× 0.6m3, JinJiuzhou, China) equipped with an electric heating system and cooling water system. The specimens were continuously softened, compressed, and fixed on the hot press. Firstly, the upper plate temperature was set at 150 ℃ and the lower plate at room temperature (25 ℃). The compression rate of 20 % was applied to samples with thicknesses of 30 mm, 40 mm, and 50 mm, resulting in compressed thicknesses of 24 mm, 32 mm, and 40 mm, respectively. Subsequently, the samples were compressed in the radial direction at a pressure of 8 MPa and a rate of 2 mm/s. After reaching the target thickness, the specimens were subjected to a pressure of 8 MPa and a temperature of 150 ℃ for 1 min. Finally, the heater switched on the upper plate was turned off, and the hot press was cooled by circulating water flow over the plates under a pressure of 2 MPa for 30 min before unloading the pressure, and concluding the experiment.

Combinations of different treatments produced 36 specimens each with a different treatment: three thicknesses of 30 mm, 40 mm and 50 mm (T30, T40, T50), three moisture content of 15 %, 25 % and 35 % (M15, M25, M35), and two conditions of sealing (sealed and unsealed samples – S and U). In total, 18 different sets were obtained with three replicates for each group.

2.3. Measurement methods

The connected thermocouples and optical fiber pressure sensors from the specimen were promptly removed, as well as the cured epoxy resin coating at the interface. The samples' weight was measured and denoted as m_c (mass of the sample after compression treatment). Subsequently, samples were sawn to obtain layer moisture content test specimen of the middle part and the end part, as well as the vertical density profile (VDP) test specimen (50 mm×50 mm (L×R), with the thickness of the test specimen after compression denoted as T_c). The weight of the layer moisture content of the middle part and the end part were measured and recorded as m_m and m_e, respectively. Additionally, the layer moisture content test specimens were split, and the weight and length of each layer were measured to calculate the layer moisture content and stress index using Eqs. 4–6. After measuring the weight and deflection of each layer, samples were placed in a blast drying oven (DHG-924OA, Yiheng Instrument Co., LTD, China) at 103 ℃ for 5 h, and the weight and deflection of each layer were remeasured. The residual stress index of each layer was calculated using Eq. 7.

$$MC_{mi} = \frac{m_{mi} - m_{mi0}}{m_{mi0}} \times 100\% \tag{4}$$

$$MC_{me} = \frac{m_{ei} - m_{ei0}}{m_{ei0}} \times 100\% \tag{5}$$

$$Y = \frac{f_i}{L_i} \times 100\% \tag{6}$$

$$Y_r = \frac{f_{ri}}{L_{ri}} \times 100\% \quad (7)$$

where MC_{mi} and MC_{me} are the moisture content of each layer (%) in the middle and at the end of the sample, respectively; m_{mi} is the weight of the i-layer at the middle of the sample, and m_{mi0} is the absolute dry weight of the i-layer at the middle of the sample after drying at 103 ℃ (kg); m_{ei} is the weight of the i-layer at the end of the sample, and m_{ei0} is the absolute dry weight of i-layer at the end of the sample; Y is the stress index of each layer (%); f_i is the deflection deformation of each layer (mm); L_i is the length of each layer (mm); Y_r is the residual stress index of each layer (%); f_{ri} is the deflection deformation of each layer after drying at 103 ℃ (mm); L_{ri} is the length of each layer after drying at 103 ℃ (mm).

Saturated steam or unsaturated superheated steam was used. The saturation temperature of water vapor under various pressures was calculated based on the Antoine equation for saturated water vapor pressure, as presented in Eq. 8.

$$T_s = \frac{B}{A - logP_a} - C \quad (8)$$

where T_s is the temperature of saturated water vapor within the wood, which is equivalent to the boiling point temperature of water at the given pressure (℃); P_a is the saturated water vapor pressure value within the wood, which is approximately equal to the actual measured wood internal gas pressure of the wood (kPa); The value of constants A, B, and C is 7.07406, 1657.46, and 227.02, respectively. If the current temperature within the wood is $T_a < T_s$, the internal water temperature of the wood will be lower than the saturated steam temperature generated under the current monitoring pressure, resulting in water in a liquid state; when $T_a = T_s$, resulting in saturated steam; and if $T_a > T_s$, resulting to superheated water vapor [24–26].

3. Results and discussion

3.1. Internal temperature distribution of wood during unilateral surface compression

As can be seen from Fig. 2, when the wood is compressed, the temperature of the surface layer (SL), the subsurface layer (SSL) and the core layer (CL) of the wood gradually increase as a function of time, until reaching a plateau value. In this study, the hot pressing time was extended to 60 min to clearly observe the changes in the wood's internal temperature and gas pressure distribution of wood. It was worth noting that in actual production, the hot pressing time was generally controlled

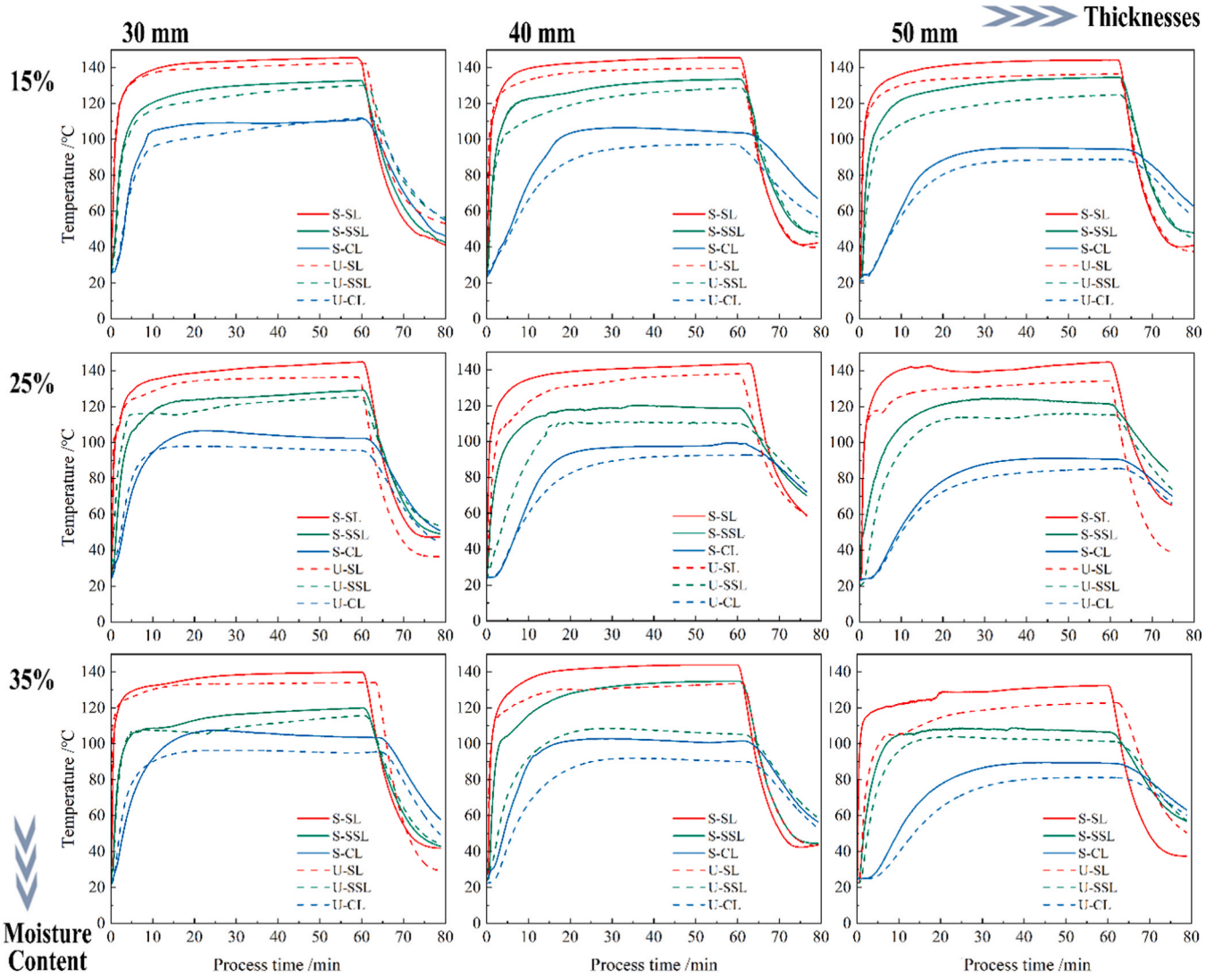

Fig. 2. Temperature profiles of the SL, SSL and CL for samples with two conditions of sealing (sealed and unsealed samples – S and U) and different moisture content (rows) and thickness (columns) during the hot pressing process.

within 30 min. Fig. 2 reveals that with an increase in hot pressing time, the SL temperature of each sample type gradually increased. However, the equilibrium temperature was reached within 60 min. Specifically, the maximum temperature of the SL was around 140 ℃, roughly 10 ℃ lower than the temperature of the hot press plate. The preparation process of surface-compressed wood relied heavily on the state of SL and SSL for successful product preparation. The results showed that there was a temperature disparity between the hot press plate temperature and the SL and SSL of the samples. Moreover, the compression area of the wood was unable to reach the temperature of the hot press plate temperature within a limited time. Therefore, the hot pressing temperature was not the highest temperature of the internal temperature of the wood.

Despite variations in the initial moisture content among samples with different thicknesses, it was observed that the maximum temperature of both the SL and the SSL remained similar. Under sealed conditions, the SL maintained a stable maximum temperature between 133 ℃ and 146 ℃, while the SSL was between 107 ℃ and 135 ℃. Similarly, under unsealed conditions, the maximum temperature of the SL was between 123 ℃ and 143 ℃, and the SSL between 97 ℃ and 130 ℃. This similarity in maximum temperature values can be attributed to the consistent distance between the SL, SSL, and CL of the wood, which allows the thermal resistance of the heat from the heating plate through these layers to have a similar thermal conductivity. Comparatively, the maximum temperature values of SL and SSL of the specimens under sealed conditions were generally higher than those under unsealed conditions. This discrepancy appeared due to the restricted moisture movement in closed conditions, limiting the heat loss. Furthermore, significant differences in the maximum temperature of the CL were observed, depending on its thickness. For example, under sealed conditions, samples with thicknesses of 50 mm, 40 mm, and 30 mm reached maximum temperatures of 95 ℃, 104 ℃, and 112 ℃, respectively. Under unsealed conditions, the peak temperatures of the CL were 89 ℃, 97 ℃, and 112 ℃, respectively. Notably, for 30 mm thick wood, the maximum temperature of the sealed and unsealed CL surpassed that of 40 mm and 50 mm thick wood by 8 ℃ to 15 ℃ and 17 ℃ and 29 ℃, respectively. This difference can be attributed to the smaller distance between the 30 mm thick of CL and the hot press plate, resulting in lower thermal resistance [27]. Additionally, compression led to a significant increase in wood density, which positively correlates with thermal conductivity.

When comparing wood samples of the same thickness but different initial moisture content, variations in the internal temperature distribution under sealed and unsealed conditions were observed. Taking 50 mm thick wood as an example, when the moisture content of the wood sample was 35 %, the SL, SSL, and CL exhibited temperature

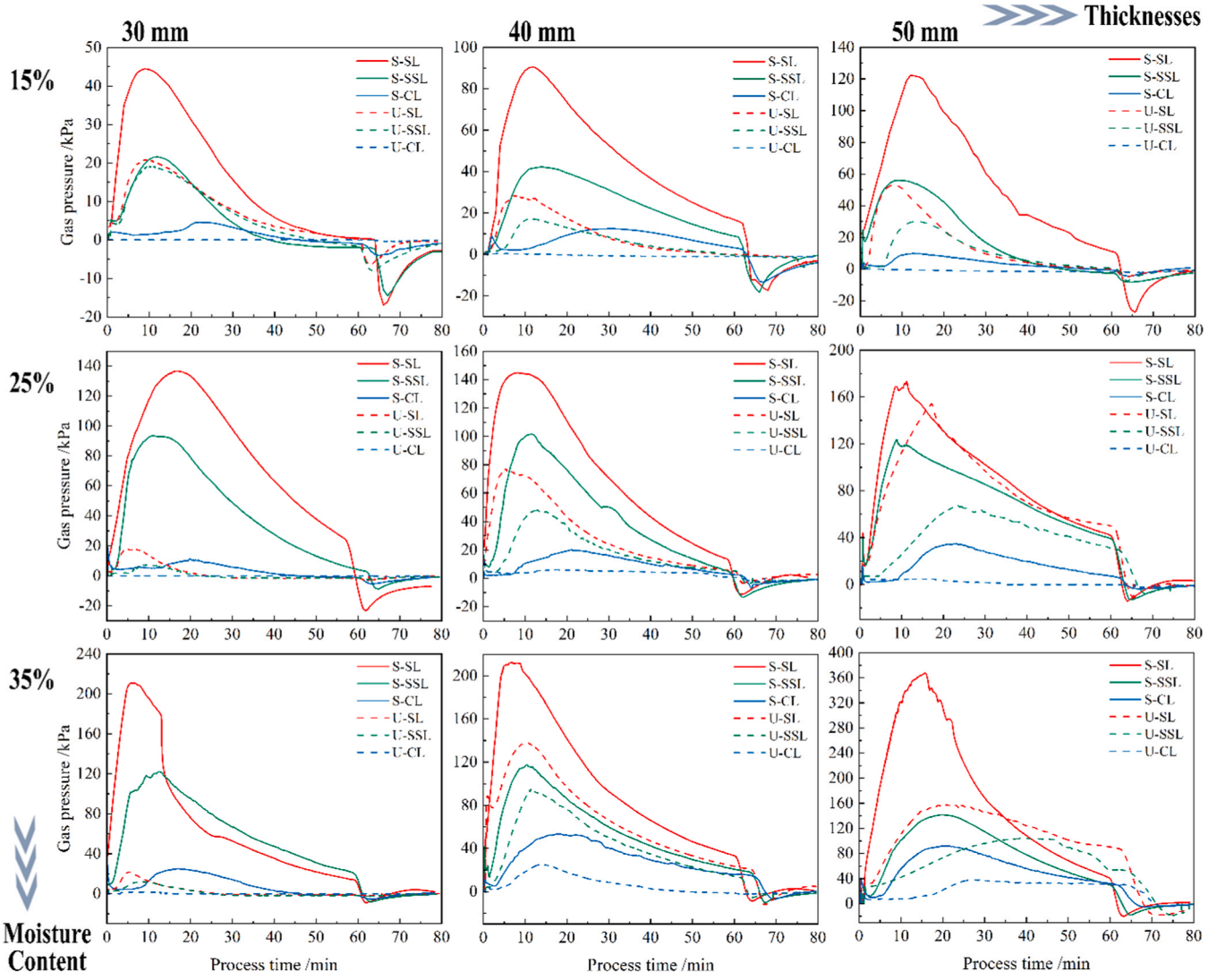

Fig. 3. Gas pressure profile of the SL, SSL and CL as a function of time for samples, with different moisture content (rows) and thickness (columns) during the hot pressing process.

values that were 10 ℃, 5 ℃, and 8 ℃ higher, respectively, under sealed conditions compared to unsealed conditions. Similarly, for wood samples with a moisture content of 25 %, the SL, SSL, and CL experienced temperature increases of 11 ℃, 6 ℃, and 5 ℃, respectively, when subject to sealed conditions. Finally, when the moisture content of the wood was 15 %, the SL, SSL, and CL exhibited temperature differences of 8 ℃, 10 ℃, and 6 ℃ higher, respectively, under sealed conditions compared to unsealed conditions. These results showed that as the initial moisture content increased, the temperature discrepancy at the same position under sealed and unsealed conditions gradually amplified.

3.2. Internal gas pressure distribution of wood during unilateral surface compression

Fig. 3 shows the evolution of the gas pressure distribution in the SL, SSL, and CL of wood during the preparation of compressed wood. As expected, in any case, the highest pressure was observed at the SL, followed by the SSL. This can be easily understood by considering that the temperature of the SL rises rapidly while is sufficiently compressed. Moreover, the higher the moisture content of the wood, the greater the amount of water vapor generated per unit of time, resulting in a maximum of gas pressure across all wood layers. When sealed, water vapor cannot escape easily, leading to a much higher gas pressure inside the wood compared to the unsealed sample. Specifically, for the same thickness and moisture content conditions, wood subjected to unsealed conditions lost approximately 2 % more mass than wood under sealed conditions. All other conditions being equal, a 10 % increase in moisture content resulted in an average gas pressure increase of 1.90 times in the SL. The microstructure analysis of poplar wood revealed that water vapor can escape through longitudinally interconnected conduits and radial pitting. Consequently, a significant amount of water vapor leakage from the radial section and cross-section of unsealed wood resulted in reduced maximum internal gas pressure. When defects such as knots were present, the situation was similar to sealing, and there was a potential risk of overpressure increase in the CL. Therefore, it was imperative to be cautious in such circumstances to avoid any damage to the sample and risk for to operator. However, the difference in gas pressure and mass loss rate for the same moisture content was not substantial. As the processing time increased, the maximum gas pressure gradually diffused toward the CL and gradually diminished. Both sealed and unsealed conditions exhibited a gas pressure maximum value sequence of SL > SSL > CL, with each layer exhibiting a successively decreasing maximum value with a delay in time. This observation indicated that water vapor migrated from the hot end to the cold end along the wood's internal porous structure under the joint influence of both temperature and gas pressure gradient, with the water vapor diffusion rate decreasing gradually during the diffusion through to the inner part of the sample.

Upon contact between the wood surface and the hot plate, the moisture near the wood surface underwent rapid vaporization. Due to the significantly larger specific volume of water vapor compared to liquid water, the vapor pressure near the wood surface experienced a rapid increase. As the compression progressed, the evaporation process moved from the wood surface towards the wood interior, driven by the vapor pressure gradient, and gradually increased the internal wood's gas pressure. Typically, high hot pressing temperatures result in greater heat transfer to the wood interior per unit of time by the hot pressing plate, leading to increased absorption of heat by the free water within the evaporation surface and, consequently, a higher proportion of water vaporization and vapor pressure formation. With greater vapor migration towards the wood interior propelled by the vapor pressure gradient, the internal water pressure shows a pronounced upward trend, resulting in higher maximum gas pressure levels [28]. Concurrently, a heat-mass coupling effect emerged, namely, as the water vapor liquefied upon reaching the cold end, the phase transition intensified the heat transfer effect. The water vapor formed in the surface part of the hot end of the wood continued to migrate towards the CL, creating a "heat vaporization-inward migration-cold liquefaction" transition process during migration. This was also proved by the layer moisture content distribution of the wood for the middle and end parts of samples after hot pressing, as shown in Fig. 4. Mass migration caused by the temperature gradient and water migration strengthened the effect of heat migration [29].

Compared to artificial panels, the variation in gas pressure distributions of unilateral surface compression exhibited significant differences during hot pressing. In this paper, at a wood moisture content of 15 %, the maximum SL pressure measured was 123.7 kPa, a value far lower than that reported by Thoemen *et al.*, despite their mat moisture content being a mere 8 % [22]. Furthermore, unilateral heating was applied in this study, and the less total heat transfer was one of the reasons for this situation. In the hot pressing process of artificial panels, the mat can be regarded as homogeneous, with internal conditions being less intricate than those of solid wood. Moreover, the maximum gas pressure value in this study lagged behind the maximum temperature value, potentially attributable to a reduction in internal free volume due to wood compression, thereby leading to an increase in internal gas pressure to a certain extent. The boiling point of free water in the wood corresponds to the saturation temperature under the prevailing water pressure. However, the saturation temperature varies with alterations in ambient pressure, with higher ambient pressure leading to a high saturation temperature. Within 5 min from the beginning of the hot pressing, both the SL and SSL temperatures were in a rapid growth stage. At this point, T_a of SSL was also lower than T_s, indicating the presence of liquid water. After 10 min, the T_a of SSL surpassed T_s, indicating water overheating in this region. This observation underscores the continual inward movement of the water evaporation within the wood, resulting in an increased gas pressure in the CL. As a result of the relatively sluggish heat conduction, the temperature of the wood CL was lower than the saturation temperature value derived from the moisture pressure measurement at the respective position.

3.3. Internal density distribution and microstructure characterization of wood

As shown in Fig. 4, the layer moisture content distribution of the wood is shown for the middle and end parts of samples with thicknesses of 50, 40, and 30 mm after hot pressing. The results indicated that upon hot pressing treatment, the moisture content of the wood near the cold end - the cold end of the hot press - was higher upon hot pressing treatment, with the range value of layer moisture content reaching 38.5 %. This suggests that the wood's internal moisture migrated from the hot end to the cold end during unilateral hot compression treatment across the entire thickness range of the wood. In all cases, regardless of the sealed or unsealed conditions, the surface moisture content of the wood was relatively low, ranging between 3 % and 5 %, indicating that moisture within an area extending 5 mm from the hot pressing surface had been almost completely transferred to the interior of the wood. For different wood thicknesses, the moisture content distribution trend inside the wood was found to be essentially the same. When the wood sample was sealed with equal thickness, the moisture content of both the middle and end parts was nearly identical, indicating a prominent sealing effect. This observation shows that moisture was evenly transferred along the thickness direction of the wood. A majority of thermo-mass coupled migration models for wood thermal processing were based on this assumption [30–32]. However, this assumption has an important premise: the wood must be standard quartersawn lumber or flatsawn lumber, so that the cut plane parallel to the direction of heat flow is homogeneous, together with the assumption of no mass exchange between the wood and external medium. When the sample was not sealed, the layer moisture content between the middle and end parts varied significantly, with the difference being more pronounced when the

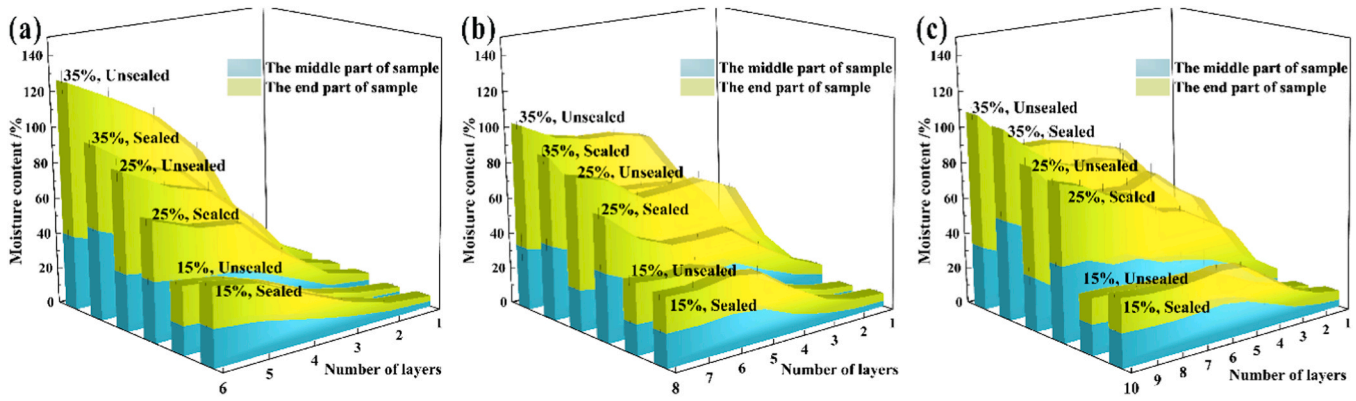

Fig. 4. Layer moisture content distribution of samples as a function of the number of layers, starting moisture content values and sealing conditions for different thicknesses after hot pressing: (a) 30 mm, (b) 40 mm, and (c) 50 mm.

sample was closer to the cold end. This occurred because the longitudinal water transmission rate in wood is several times higher than in the radial direction [33], and in the unsealed state, moisture will migrate to the end surface through the lumina and other tissues, spreading from the end surface to the external environment. Consequently, a large amount of moisture accumulates at the end.

Wood is a natural anisotropic solid foam whose solid matrix is a macromolecular composite with complex viscoelastic and viscoplastic behavior [34,35]. Dry wood can be plasticized by moisture and heat, therefore, the moisture content and temperature of each layer are closely related to the degree of softening affecting the region and location of the dense layer. During the thermal compression treatment process, wood shows a stepped distribution, forming regions with glassy and elastic states with high mobility polymers due to the presence of plasticizers and high temperature. When subjected to pressure, the plastic domains – and the elastic domains to a lesser extent - near the hot end deformed resulting in the formation of a high-density compressed region which retained the new shape upon cooling. Fig. 5 illustrates the vertical density profile of samples with different thicknesses. It was evident that samples with higher moisture content exhibited a larger densification region due to a higher plasticization effect when more water was available in the tissue and, therefore, a higher deformation could be achieved [36]. Wood samples of different thicknesses displayed the same density structure under identical process parameters. However, the influence of compressed thickness in the densification area varied. As a result, the same compression process can be applied to woods of different thicknesses while maintaining a consistent maximum density structure, which holds significant importance in practical production.

Fig. 6 illustrates sample's appearance in the densified area with 15 %, 25 % and 35 % moisture content. As shown there, the vessel elements and ray cells within wood can be identified as stress concentration sites due to their susceptibility to deformation. Specifically, the ray cells of the sample with a moisture content of 15 % exhibited migration and compression, displaying a closely fitting state. In contrast, the fiber cells within wood demonstrated greater resilience to stress, exhibiting minimal deformation. Furthermore, a noticeable trend was observed as the moisture content decreased, leading to a reduction in pore size and a denser wood structure in the compressed wood. This trend solidified the findings from Fig. 5, in the 1–2 mm region, samples with low moisture content exhibit a higher level of densification, while the opposite holds true for samples within the 2–5 mm range. This phenomenon is likely attributable to the propensity for the surface layer of low moisture samples to soften more readily than the interior. Moreover, an increase in moisture content amplifies the softening effect, reducing the glass transition temperature. Based on our current process, the dense-layer is an area around 5 mm away from the compressed surface. If there is a low moisture content density within 1 mm, the corresponding density in other areas will be diminished. Therefore, moisture content, preheating time, and compression speed are distinct parameters, they may at times yield similar effects. In the case of the sample with 15 % moisture content, the pressure was primarily concentrated on the surface of the hot press plate in contact with the wood, hindering its transfer and dispersion [37]. As a result, the surface of the wood bore more pressure, leading to an increase in surface density.

3.4. The layer stress and layer residual stress distribution

Following wood compression, Fig. 7 shows that the first three layers exhibited a high-stress index, with stress being concentrated in these regions. After drying at 103 ℃ for 3 h, the residual stress index of the second, third, and fourth layers became larger, as shown in Fig. 8. By

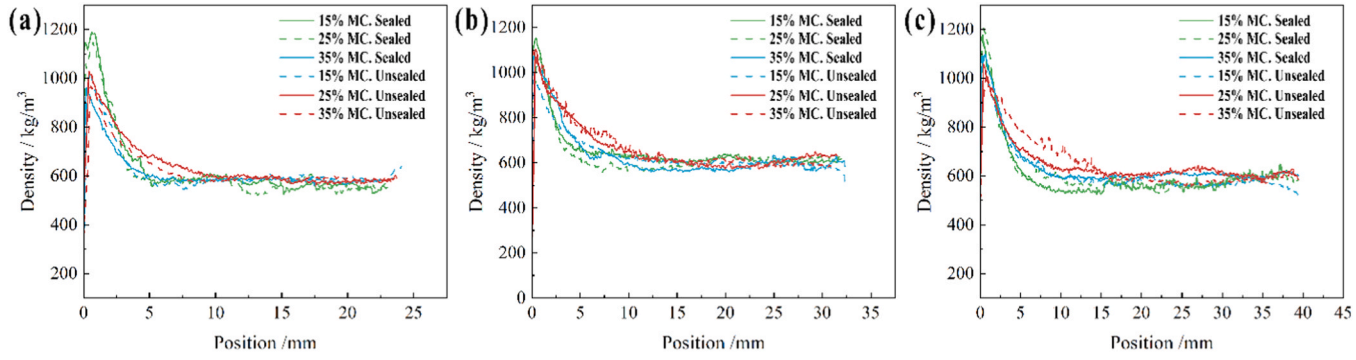

Fig. 5. Vertical density profiles of samples with different starting moisture content (MC) values and sealing conditions for different thicknesses after hot pressing: (a) 30 mm, (b) 40 mm, and (c) 50 mm.

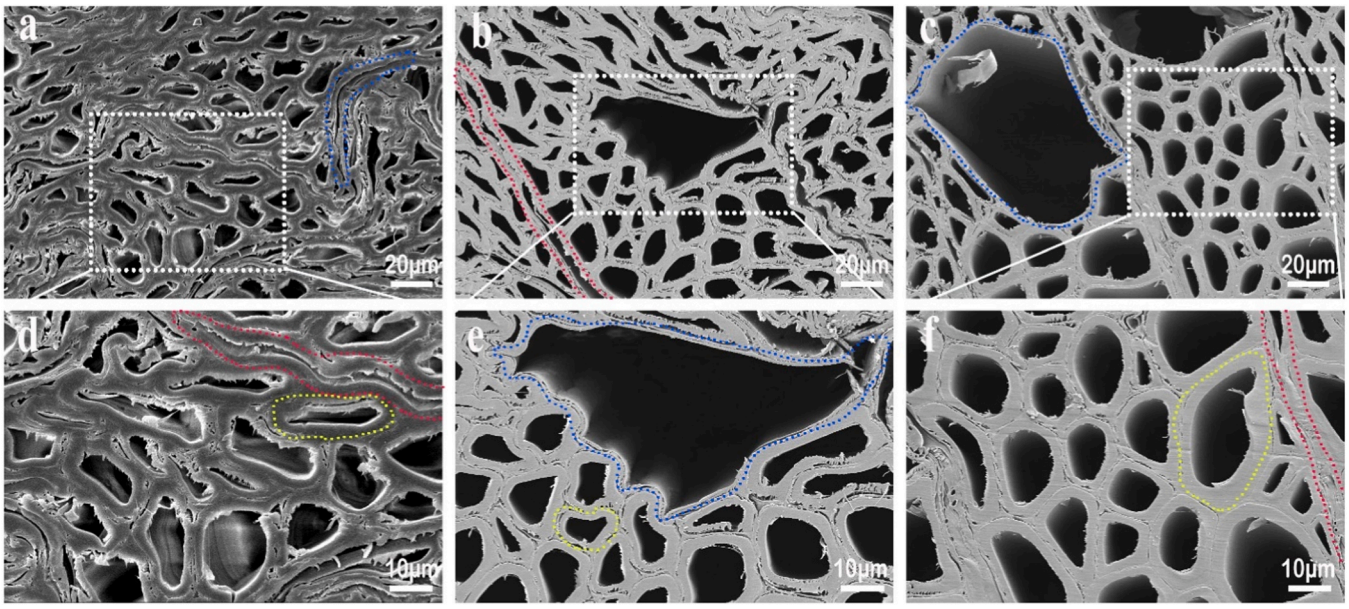

Fig. 6. SEM micrographs of samples in the densified area with 15 % (a and d), 25 % (b and e), and 35 % (c and f) moisture content. The ray cells, fiber cells and vessels are marked by red, yellow and blue dotted lines, respectively.

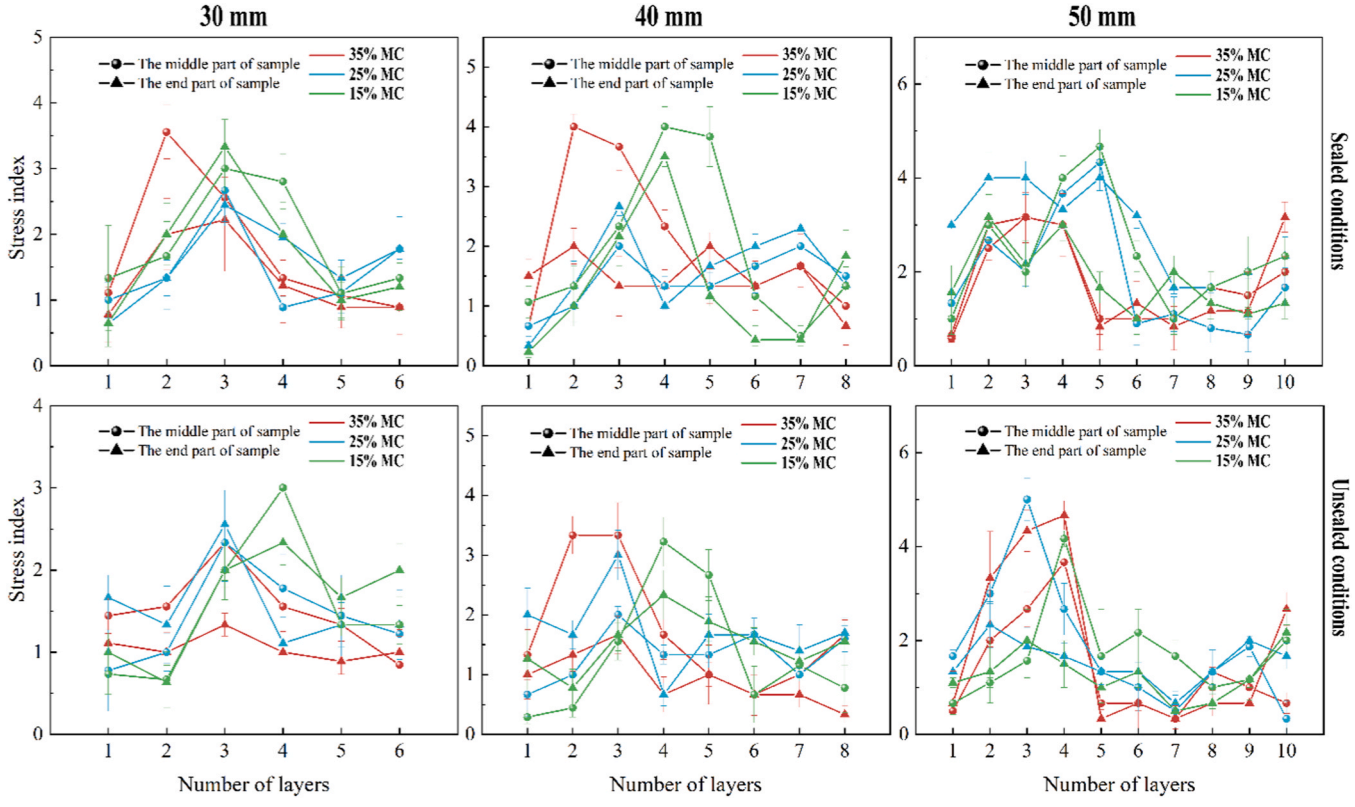

Fig. 7. The layer stress index distribution of the samples for different moisture content (MC) values and thicknesses after hot pressing.

splitting the middle and end parts and obtaining stress sections, it was observed that stress sections from the first three layers bent rapidly in the opposite direction of compression before drying, while after drying, each layer in the stress section bent in the direction of compression. Following the VDP approach, the first layer of samples from each thickness value experienced complete compaction, thereby forming a dense region. The second, third, and fourth layers underwent partial compaction and served as transitional regions. The fifth layer remained uncompressed. Moisture within the densification region migrated inwards, leading to a reduced moisture content below the fiber saturation point and consequent dry shrinkage appeared. Meanwhile, the moisture content of each layer remained higher than the fiber saturation point due to moisture migration in the sample, thereby maintaining an unchanged size and morphology. As a result, the densified region was exposed to tensile stress inside the wood, while the wood interior experienced compressive stress inside the densified region [38].

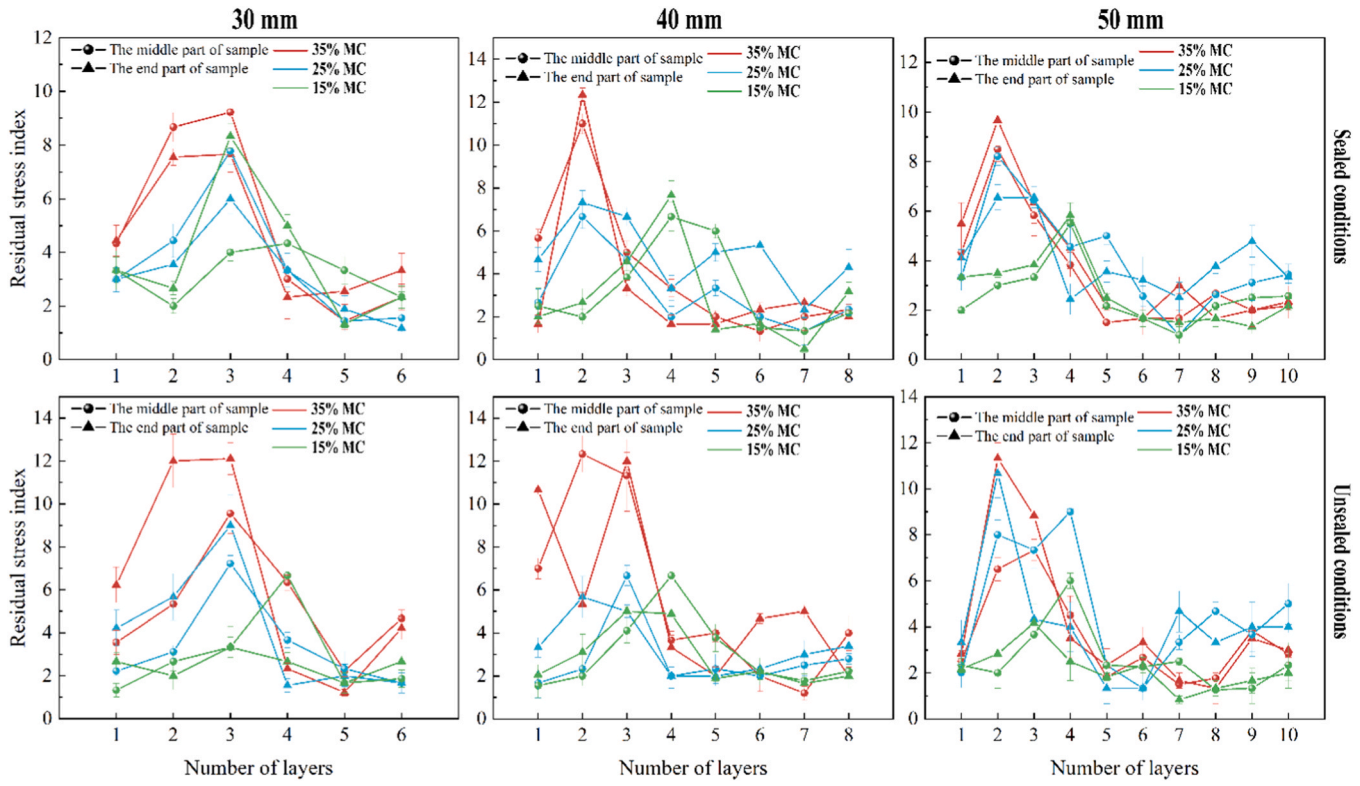

Fig. 8. The layer residual stress index distribution of the samples for different moisture content (MC) values and thicknesses after drying at 103 ℃ for 3 h.

After sectioning, the removal of tensile stress and the disappearance of elastic tensile strain within the densified layer area led to its contraction due to dry shrinkage, resulting in a macroscopic reverse crooking in the direction of the compression force. Conversely, the elimination of compressive stress within the densified region caused the elastic compressive strain in the wood interior to revert to its original length, resulting in a macroscopic curvature in the direction of compression force. With the elimination of moisture content differences, the densified region underwent plastic fixation due to compression, effectively halting further drying shrinkage within this region. However, the excessive region, which was insufficiently compressed, exhibited varying degrees of creep. Following drying, the densified region exhibited a small dry shrinkage coefficient, while the un-densified region exhibited a large dry shrinkage coefficient, presenting a macroscopic crooking in the direction of compression force. Furthermore, since the un-densified region could freely shrink after reducing moisture content, it also displayed the macroscopic manifestation of the compression force direction. The transition area, which served as the connecting region between the densified and un-densified areas, exhibited a concentration of residual stress and consequently became prone to deformation. While it was commonly believed that stress concentration in the densified area was the primary cause for delayed deformation in compressed wood, the results of this study showed that the main cause resided within the transition area rather than the densified area. The presence of internal stress in wood was identified as the direct cause of deformation during storage and post-processing, with the uneven distribution of internal moisture content serving as the underlying source of stress. Hence, it was feasible to regulate moisture redistribution by employing the temperature difference method to adjust the cold and hot ends.

4. Conclusions

In summary, this paper investigated the influence of wood moisture content, wood thickness, and sealing conditions on the internal temperature and gas pressure of wood during hot pressing. It was found that the maximum temperature values of the SL and SSL of wood with different thicknesses were similar. Moreover, under sealed conditions, SL and SSL temperatures were generally 6 ℃ to 7 ℃ higher compared to unsealing conditions. With respect to gas pressure, the maximum value followed the order: SL > SSL > CL. The gas pressure maximum value exhibited an opposite order, gradually transferring to the CL and declining as the processing time extended. The liquid-free water within the wood was expected to be in a state of overpressure saturation. Under the sealed conditions, mass loss rates were significantly lower, while internal gas pressure was 1–2 times higher than under open conditions. During compression treatment, water within the wood migrated from the hot end to the cold end. The moisture content displayed significant differences between the middle and end parts of the wood under unsealed conditions, with the disparity becoming more pronounced further away from the hot end. The transition region of the compressed wood served as a stress concentration area, experiencing the highest levels of stress. The dense region followed with the second highest stress levels, while the un-densified region exhibited the least amount of stress. The utilization of the temperature difference method to control water redistribution and prevent deformation in compressed materials will be the primary focus of future research.

CRediT authorship contribution statement

Zhipeng Zhu: Writing – original draft, Software, Methodology, Investigation, Data curation. **Xiaoxue Song:** Formal analysis. **Xiang Chi:** Software. **Jingyao Zhao:** Investigation, Formal analysis, Conceptualization. **Qiaofang Zhou:** Investigation, Conceptualization. **Antoni Sanchez-Ferrer:** Data curation, Writing – review & editing. **Dengyun Tu:** Writing – review & editing, Project administration, Funding acquisition, Conceptualization. **Wanli Cheng:** Writing – review & editing, Investigation, Conceptualization.

Declaration of Competing Interest

The authors declare that they have no known competing financial interests or personal relationships that could have appeared to influence the work reported in this paper.

Data Availability

Data will be made available on request.

Acknowledgements

This work was supported by the National Natural Science Foundation of China (No. 32271786), the Innovation Foundation for Doctoral Program of Forestry Engineering of Northeast Forestry University (No. LYGC202104), the Natural Science Foundation of Guangdong Province (No. 2023A1515012119) and the Fundamental Research Funds for the Central Universities (No. 2572023AW54).

Appendix A. Supporting information

Supplementary data associated with this article can be found in the online version at doi:10.1016/j.conbuildmat.2024.137099.

References

[1] J. Parviainen, G. Frank, Protected forests in Europe approaches-harmonising the definitions for international comparison and forest policy making, J. Environ. Manag. 67 (1) (2003) 27–36, https://doi.org/10.1016/s0301-4797(02)00185-8.
[2] P.J. Verkerk, G. Zanchi, M. Lindner, Trade-offs between forest protection and wood supply in Europe, Environ. Manag. 53 (6) (2014) 1085–1094, https://doi.org/10.1007/s00267-014-0265-3.
[3] R. Li, Z. Gao, S. Feng, J. Chang, R. Huang, Effects of preheating temperatures on the formation of sandwich compression and density distribution in the compressed wood, Eur. J. Wood Wood Prod. 64 (4) (2018), https://doi.org/10.1007/s10086-018-1758-0.
[4] D. Tu, W. Fan, Q. Zhou, Thermo-mechanical densification of *Populus tomentosa var. tomentosa* with low moisture content, Bioresources 9 (3) (2014) 3846–3856, https://doi.org/10.15376/biores.9.3.3846-3856.
[5] Y. Zhang, P. Guan, Y. Zuo, P. Li, X. Bi, X. Li, Preparation of highly-densified modified poplar wood by evacuating the micro-pores of wood through a gas expansion method, Ind. Crops Prod. 194 (2023) 9, https://doi.org/10.1016/j.indcrop.2023.116374.
[6] X. Zhang, Q. Fan, C. Chen, X. Hao, Z. Liu, R. Ou, Q. Wang, Enhanced mechanical performance and fire resistance of poplar wood: unilateral surface densification assisted with N/P doped acrylic resin impregnation, Constr. Build. Mater. 398 (2023), https://doi.org/10.1016/j.conbuildmat.2023.132470.
[7] J. Wang, Y. Yao, Y. Huang, Y. Ma, J. Xi, X. Wang, H. Li, Z. Yang, Effects of the combination of compression and impregnation with phenolic resin on the dimensional stability in the multiscale wood structure of Chinese fir, Constr. Build. Mater. 327 (2022), https://doi.org/10.1016/j.conbuildmat.2022.126960.
[8] S. Augustina, W. Dwianto, I. Wahyudi, W. Syafii, P. Gérardin, S. Marbun, Wood impregnation in relation to its mechanisms and properties enhancement, Bioresources 18 (2) (2023) 4332–4372, https://doi.org/10.15376/biores.18.2.Augustina.
[9] M. Jakob, I. Czabany, S. Veigel, U. Müller, W. Altmutter, Comparing the suitability of domestic spruce, beech, and poplar wood for high-strength densified wood, Eur. J. Wood Wood Prod. 80 (4) (2022) 859–876, https://doi.org/10.1007/s00107-022-01828-0.
[10] D. Tu, C. Chen, Q. Zhou, R. Ou, X. Wang, Research progress of thermo-mechanical compression techniques for wood products, J. For. Eng. 6 (1) (2021) 13–20, https://doi.org/10.13360/j.issn.2096-1359.202001036.
[11] B. Kuai, Z. Wang, J. Gao, J. Tong, T. Zhan, Y. Zhang, J. Lu, L. Cai, Development of densified wood with high strength and excellent dimensional stability by impregnating delignified poplar by sodium silicate, Constr. Build. Mater. 344 (2022), https://doi.org/10.1016/j.conbuildmat.2022.128282.
[12] J. Wu, Q. Fan, Q. Wang, Q. Guo, D. Tu, C. Chen, Y. Xiao, R. Ou, Improved performance of poplar wood by an environmentally-friendly process combining surface impregnation of a reactive waterborne acrylic resin and unilateral surface densification, J. Clean. Prod. 261 (2020), https://doi.org/10.1016/j.jclepro.2020.121022.
[13] D. Sandberg, P. Haller, P. Navi, Thermo-hydro and thermo-hydro-mechanical wood processing: An opportunity for future environmentally friendly wood products, Wood Mater. Sci. Eng. 8 (1) (2013) 64–88, https://doi.org/10.1080/17480272.2012.751935.
[14] N. Meyer, H. Thoemen, Gas pressure measurements during continuous hot pressing of particleboard, Holzforschung 65 (1) (2006) 49–55, https://doi.org/10.1007/s00107-006-0140-x.
[15] D. Tu, Q. Zhou, Solid wood compression, Chemical Industry Press, Beijing, 2021.
[16] Y. Zhou, J. Hou, Moisture state and migration mechanism of high moisture content poplar lumber during platen drying, Sci. Silvae Sin. 56 (9) (2020) 104–111, https://doi.org/10.11707/j.1001-7488.20200912.
[17] C. Chen, D. Tu, Q. Zhou, J. Zhou, X. Wang, B. Cherdchim, R. Ou, Development and evaluation of a surface-densified wood composite with an asymmetric structure, Constr. Build. Mater. 242 (2020), https://doi.org/10.1016/j.conbuildmat.2020.118007.
[18] Z. Zhu, Q. Zhou, W. Cheng, J. Zhao, D. Tu, Effect of unilateral surface compression technique and heat treatment on industrial application performance of poplar, Ind. Crops Prod. 211 (2024), https://doi.org/10.1016/j.indcrop.2024.118287.
[19] Q. Zhou, C. Chen, D. Tu, Z. Zhu, K.J.B. Li, Surface densification of poplar solid wood: effects of the process parameters on the density profile and hardness, BioResources 14 (2) (2019) 4814–4831, https://doi.org/10.15376/biores.14.2.4814-4831.
[20] D. Tu, X. Su, T. Zhang, W. Fan, Q. Zhou, Thermo-mechanical densification of Populus tomentosa var. tomentosa with low moisture content, BioResources 9 (3) (2014) 3846–3856, https://doi.org/10.15376/biores.9.3.3846-3856.
[21] P. Humphrey, A. Bolton, The hot pressing of dry-formed wood-based composites - Part V. The effect of board size: comparability of laboratory and industrial pressing, Holzforschung 43 (6) (1989) 401–405, https://doi.org/10.1515/hfsg.1989.43.6.401.
[22] A. Steffen, H. ThoÈmen, P. Humphrey, Temperature and gas pressure in MDF-mats during industrial continuous hot pressing, Holzforschung 57 (1999) 154–155, https://doi.org/10.1007/s001070050033.
[23] Z. Liu, B. Zhang, H. He, Variation property of steam pressure and temperature in wood during microwave drying, J. B. For. Univ. 28 (6) (2006) 124–127, https://doi.org/10.3321/j.issn:1000-1522.2006.06.022.
[24] L. Wang, X. Chen, Y. Zhu, X. Wei, Z. Tong, Indirect experimental method for measuring liquid component saturated vapour pressure of natural product, Chem. Res. Appl. 20 (9) (2008) 1121–1124, https://doi.org/10.1007/s11670-008-0115-z.
[25] F. Fang, Z. Wu, Parameter regression in the mathematical relation of vapor pressure and temperature, J. H. Univ. 23 (4) (2003) 402–406, https://doi.org/10.3969/j.issn.1000-1565.2003.04.016.
[26] X. Tang, M. Zhang, H. Zhao, L. Zhou, X. Chen, The temperature-pressure relationship of mixed gases in the autoclave, Microbiology 30 (3) (2003) 14–17, https://doi.org/10.3969/j.issn.0253-2654.2003.03.004.
[27] M. Chen, K. Semple, Ya Hu, J. Zhang, C. Zhou, H. Pineda, Y. Xia, W. Zhu, C. Dai, Fundamentals of bamboo scrimber hot pressing: mat compaction and heat transfer process, Constr. Build. Mater. 412 (2024), https://doi.org/10.1016/j.conbuildmat.2023.134843.
[28] A. Bakkour, S. Ouldboukhitine, P. Biwole, S. Amziane, A review of multi-scale hygrothermal characteristics of plant-based building materials, Constr. Build. Mater. 412 (2024), https://doi.org/10.1016/j.conbuildmat.2023.134850.
[29] B. Zhang, S. Yi, X. Cui, Characteristics of moisture movement on wood dried under vacuum superheated steam, J. Eng. Thermophys. 23 (1) (2002) 169–172, https://doi.org/CNKI:SUN:GCRB.0.2002-S1-043.
[30] P. Wang, P. Li, Y. Tao, Study on Hheat transfer model and visualization of numerical algorithm about wood veneer during hot-pressing, Trans. Mater. Heat. Treat. 26 (1) (2005) 90–92, https://doi.org/10.3969/j.issn.1009-6264.2005.01.022.
[31] D. Kocaefe, R. Younsi, B. Chaudry, Y. Kocaefe, Modeling of heat and mass transfer during high temperature treatment of aspen, Wood Sci. Technol. 40 (5) (2006) 371–391, https://doi.org/10.1007/s00226-006-0069-6.
[32] L. Czajkowski, W. Olek, J. Weres, R. Guzenda, Thermal properties of wood-based panels: thermal conductivity identification with inverse modeling, Eur. J. Wood Wood Prod. 74 (4) (2016) 577–584, https://doi.org/10.1007/s00107-016-1021-6.
[33] A. Sánchez-Ferrer, M. Engelhardt, K. Richter, Anisotropic wood–water interactions determined by gravimetric vapor sorption experiments, Cellulose 30 (6) (2023) 3869–3885, https://doi.org/10.1007/s10570-023-05093-z.
[34] B. Toson, P. Viot, J.J. Pesqué, Finite element modeling of Balsa wood structures under severe loadings, Eng. Struct. 70 (2014) 36–52, https://doi.org/10.1016/j.engstruct.2014.03.017.
[35] T. Fothe, U.G. Azeufack, B. Kenmeugne, M. Fogue, A one-dimensional elasto-viscoplastic model coupled to damage for the description of creep in wooden materials, J. Wood Sci. 68 (1) (2022), https://doi.org/10.1186/s10086-022-02015-8.
[36] S. Zhao, W. Zhang, F. Meng, J. Wei, Y. Bao, N. Li, F. Lin, Z. Wang, M. Bao, Effect of thermo-mechanical treatment with different initial moisture content on bamboo cell walls, Constr. Build. Mater. 411 (2024), https://doi.org/10.1016/j.conbuildmat.2023.134801.
[37] Y. Wu, R. Huang, Z. Gao, The relationship between the hydrothermal response of yield stress and the formation of sandwich compressed wood, J. Sandw. Struct. Mater. 24 (1) (2022) 101–118, https://doi.org/10.1177/1099636221993870.
[38] J. Wang, X. Wang, Q. He, Y. Zhang, T. Zhan, Time-temperature-stress equivalence in compressive creep response of Chinese fir at high-temperature range, Constr. Build. Mater. 235 (2020), https://doi.org/10.1016/j.conbuildmat.2019.117809.